

Supporting Information

Modulation of Electrophoresis, Electroosmosis and Diffusion for Electrical Transport of Proteins through a Solid-State Nanopore

Jugal Saharia¹, Y. M. Nuwan D. Y. Bandara¹, Buddini I. Karawdeniya¹, Cassandra Hammond¹, George Alexandrakis², and Min Jun Kim^{1,*}

¹Department of Mechanical Engineering, Southern Methodist University, Dallas, TX 75275, U.S.A.

²Department of Bioengineering, University of Texas at Arlington, Arlington, TX 76019, U.S.A.

Corresponding Authors: mjkim@lyle.smu.edu

Table of Contents

Section 1: Lowpass Filtering and the Translocation Time	2
Section 2: Current Traces	3
Section 3: Gaussian Fitting of ΔG_{hSTf} Distribution	9
Section 4: ζ_{pore} , σ_{hSTf} and Electrolyte Concentration	12
Section 5: Quantification of Capture Rate	13
Section 6: Derivation of Equation 5	15
References	19

Section 1: Lowpass Filtering and the Trasnlocation Time

The rise-time of the lowpass filter can be written as

$$T_r = 0.3321/f_c \quad \text{Eq. S1}$$

where f_c is the cutoff frequency of the filter. Events with trasnlocation time $< 2T_r$ are known to be seriously attenuated which is $\sim 66 \mu\text{s}$ ($f_c=10 \text{ kHz}$) in our case. Here we used a calibration method where the Axopatch 200B (Molecular Devices, USA) was fed with square-pulses of known height (ΔI_{func}) and width (τ_{func}) using a function generator (HP 33120a). The data were filtered using the in-built Bessel low-pass filter of the Axopatch 200B at 10 kHz and recorded using a Digidata Digitizer at a sampling frequency of 250 kHz. The trasnlocation time (τ_{cal}) was calculated using a custom MATLAB script (R2020b) using the two sides of the blockade method (TSB, Figure S1, magenta points) and full width at half maximum (FWHM, Figure S1, blue points) methods.¹ The ideal trend of t_{func} with τ_{cal} is shown by the black fitline of Figure S1 (slope =1) where we see a close agreement with the values calculated by the FWHM method whereas the TSB clearly over estimates the pulse width as previously observed by *Pedone et al.*¹

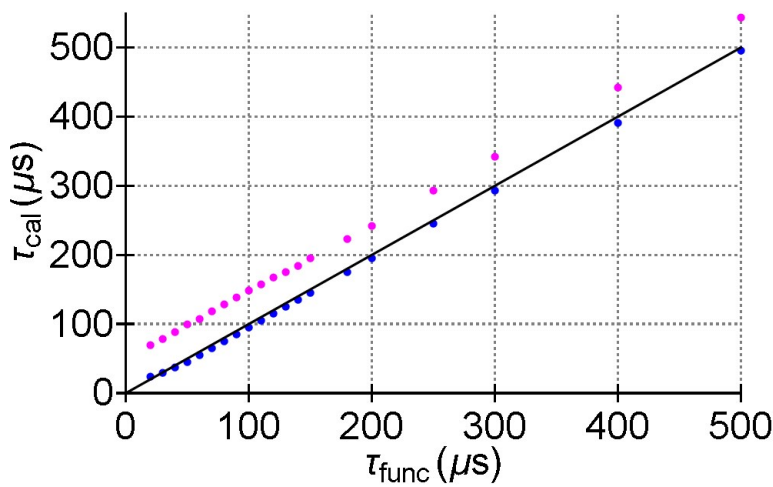


Figure S1: A plot of t_{func} against τ_{cal} calculated using the two side of the blockade method (magenta)

and the full width at the half maximum (FWHM) method (blue). The ideal trend is depicted by the solid black fitline (slope =1).

Section 2: Current Traces

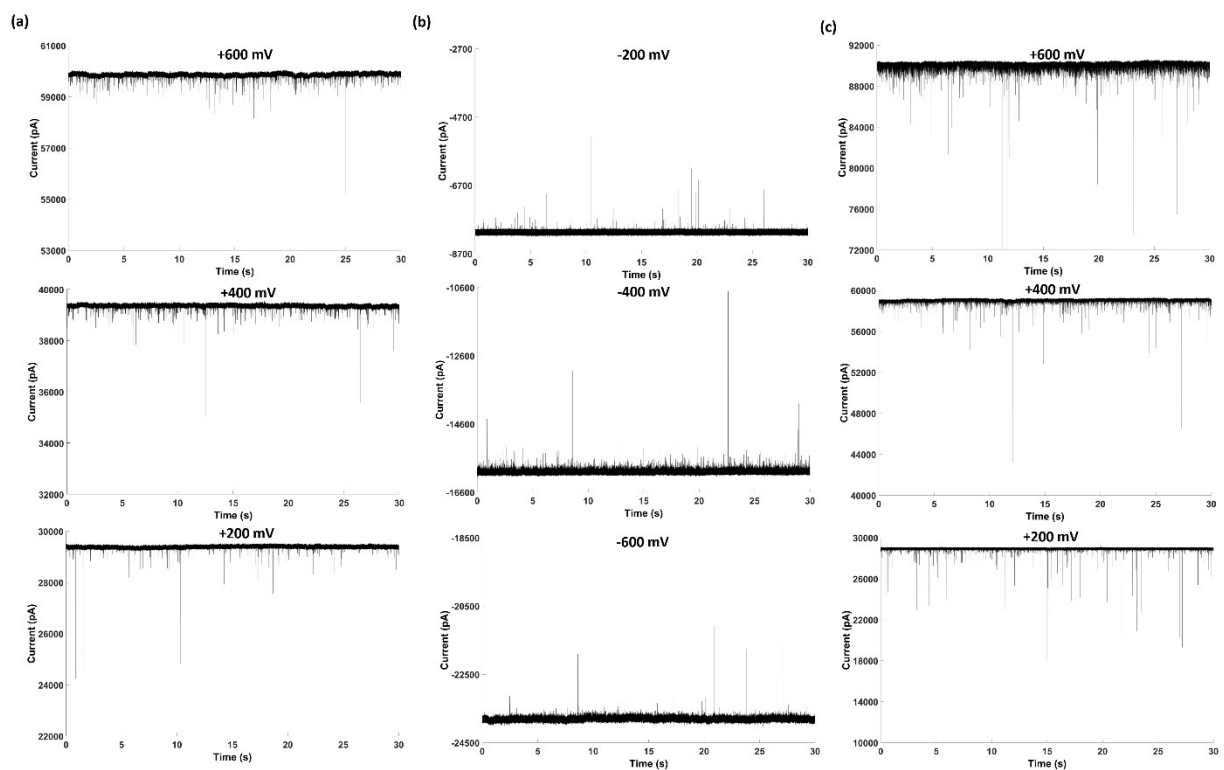


Figure S2: Current traces (30 s) corresponding to hSTf in (a) 4M LiCl, (b) 1M LiCl and (d) 2M KCl under applied voltages noted on each of the figure panels. All electrolytes were buffered at pH ~8.

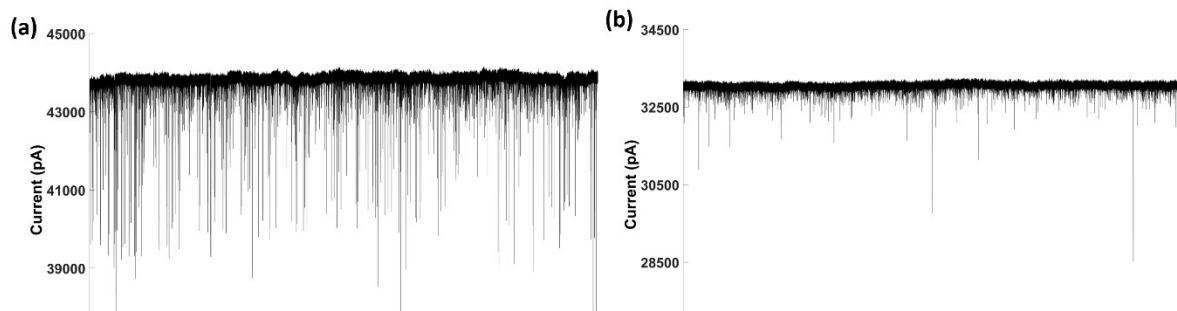


Figure S3: Extended current traces (100 s) corresponding to hSTf in **(a)** 4M LiCl, **(b)** 3M LiCl **(c)** 2.5M LiCl and **(d)** 2M LiCl under an applied voltage of +400 mV at pH ~8

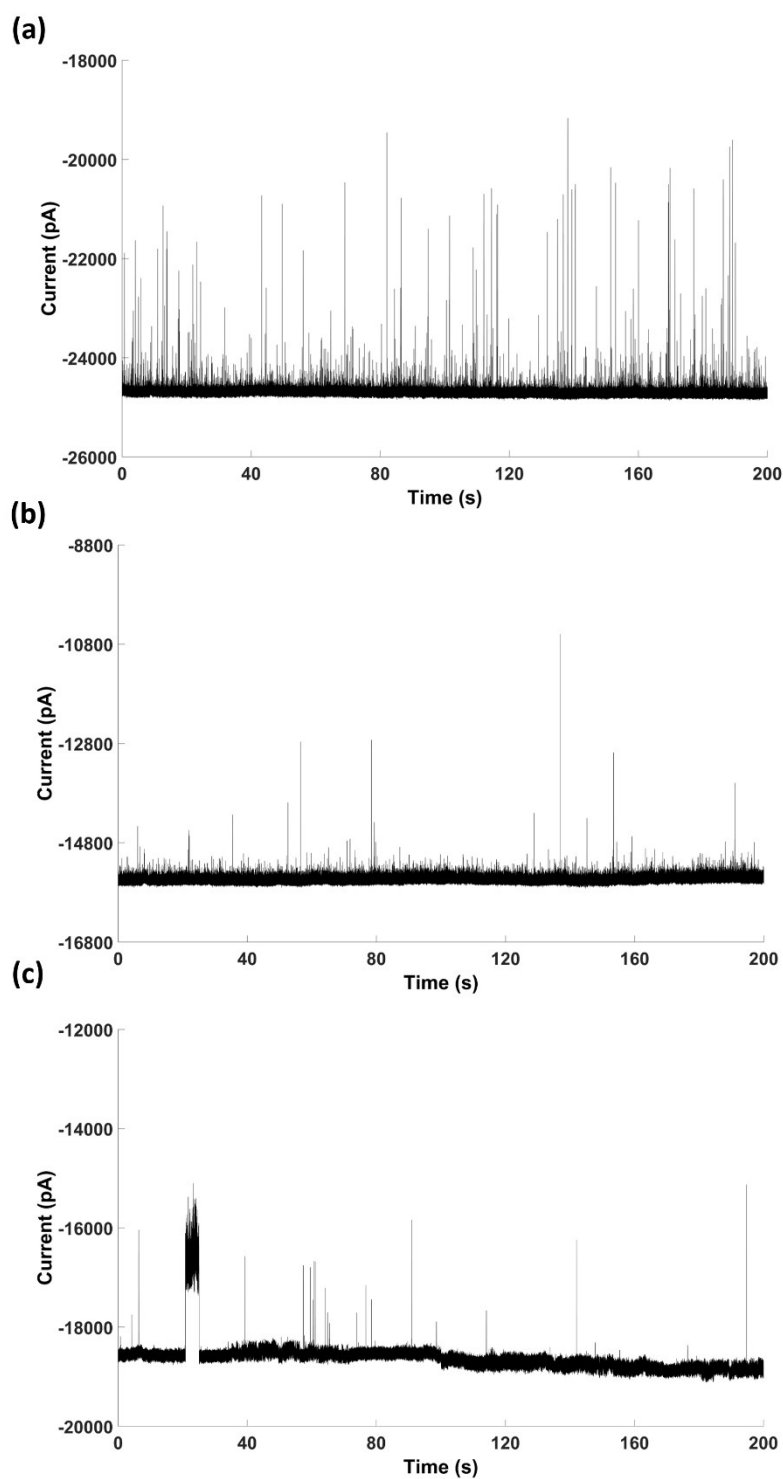


Figure S4: Extended current traces (200 s) corresponding to hSTf in (a) 1.5M LiCl, (b) 1M LiCl, and (c) 0.5M LiCl under an applied voltage of -400 mV at pH ~8

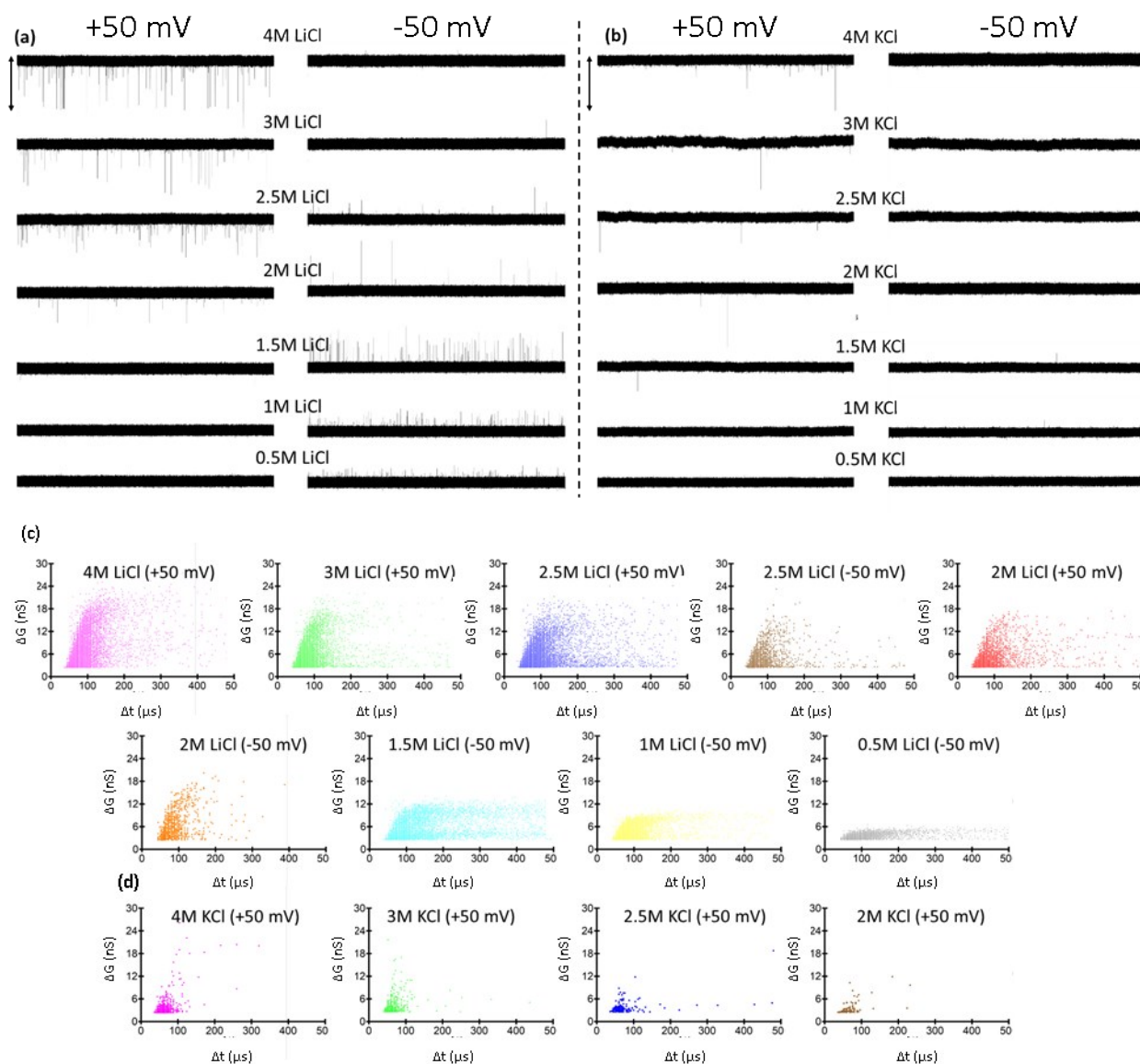


Figure S5: 25-second current traces corresponding to hSTf translocations in (a) LiCl and (b) KCl under (left column) +50 mV and, (right column) -50 mV of applied voltage at pH ~8. The vertical bar at the top corresponds to 1000 pA. Scatter plots corresponding to change in conductance as a result of analyte

transit with the corresponding translocation time for 4M, 3M, 2.5M, 2M, 1.5M, 1M and 500 mM of (c) LiCl and (d) 4M, 3M, 2.5M and, 2M KCl buffered at pH ~8. All experiments were conducted using ~14 nm diameter pores.

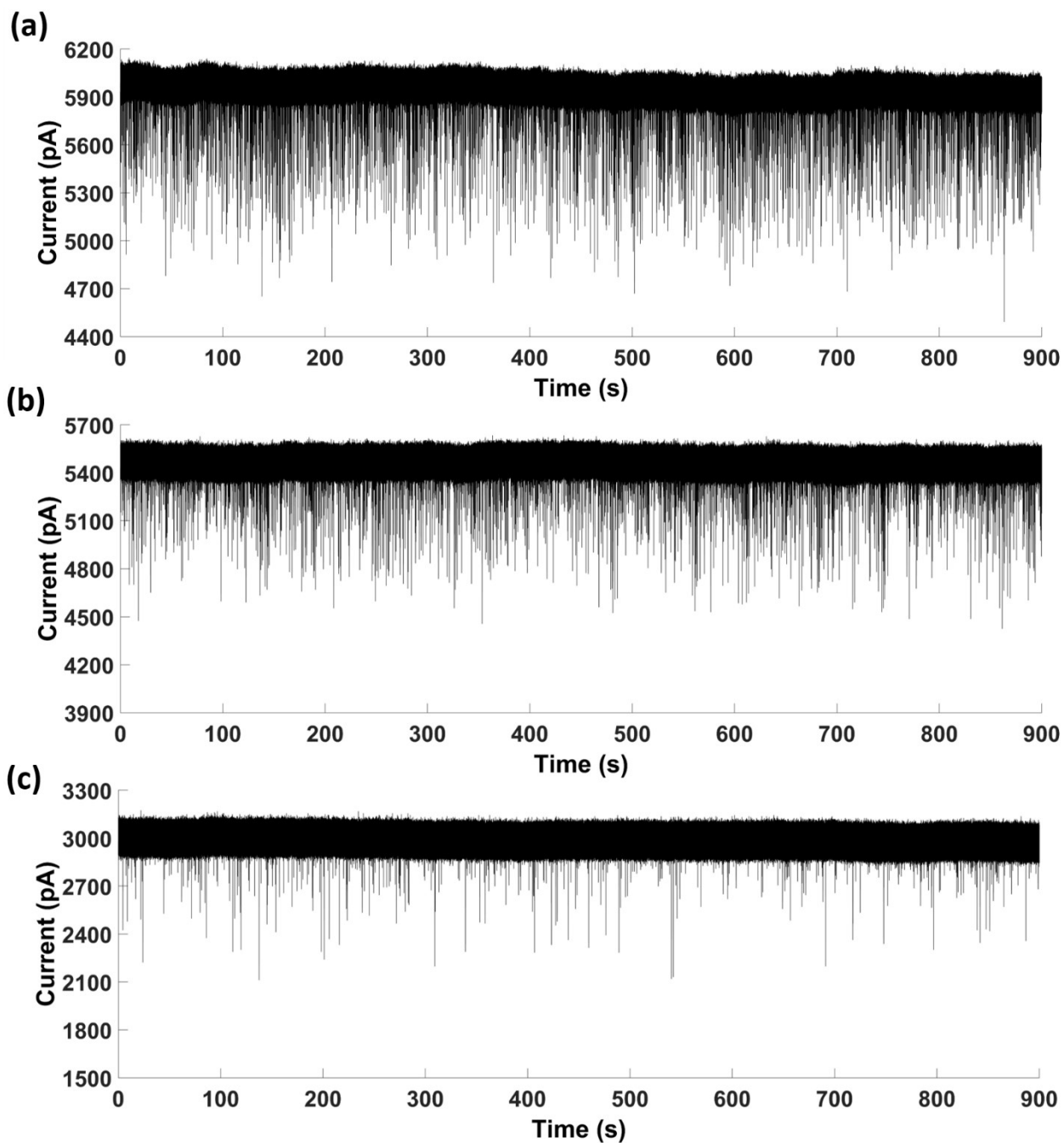


Figure S6: Extended current traces (900 s) corresponding to hSTf in (a) 4M LiCl, (b) 3 M LiCl and

(c) 2M LiCl under an applied voltage of +50 mV at pH ~8

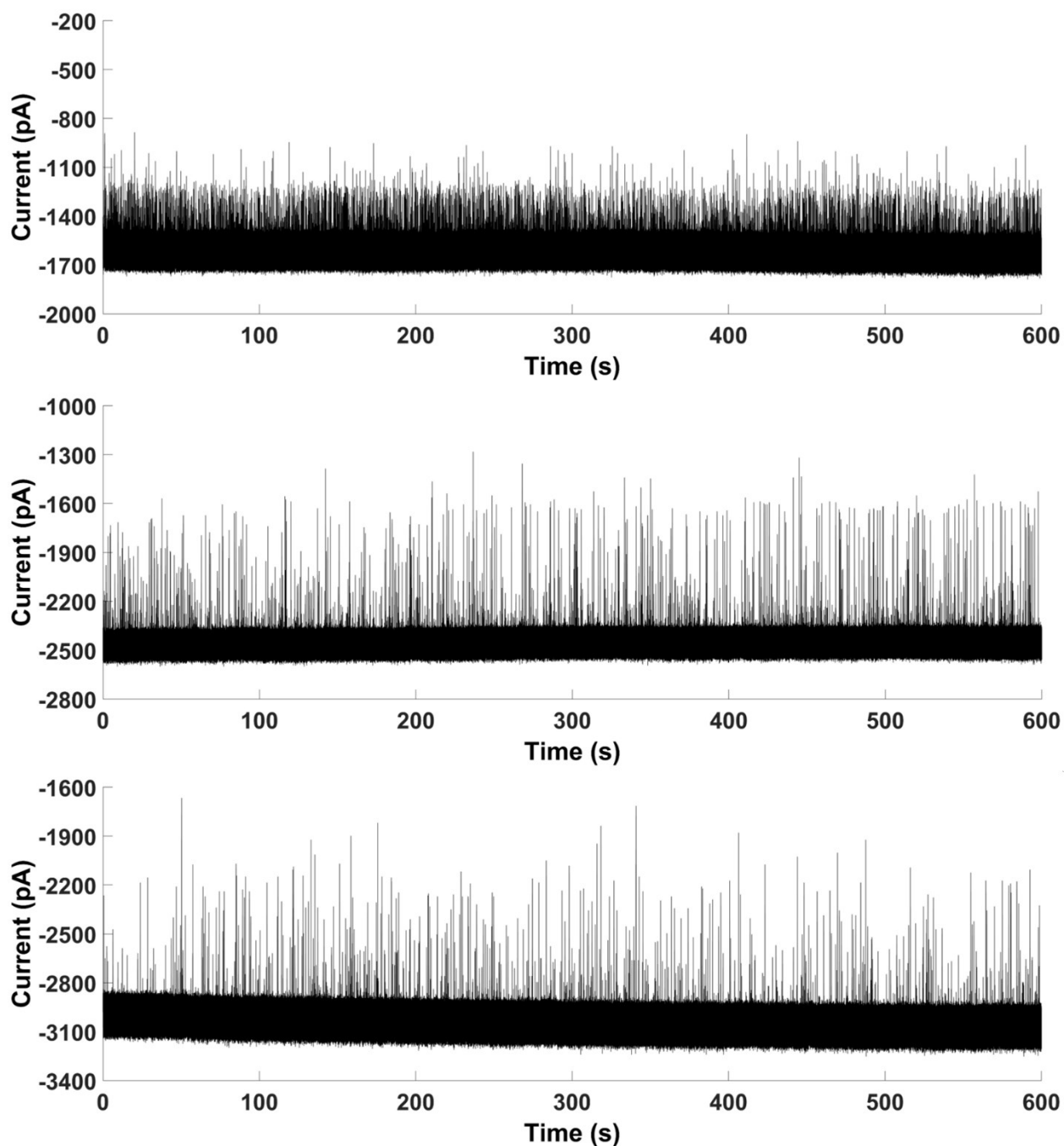


Figure S7: Extended current traces (600 s) corresponding to hSTf in (a) 0.5M LiCl, (b) 1M LiCl and (c) 1.5M LiCl under an applied voltage of -50 mV at pH ~8

Section 3: Gaussian Fitting of ΔG_{hSTf} Distribution

$$A_i \exp\left(-(\Delta I_i - \mu_i)^2 / \sigma_i^2\right) \quad \text{Eq. S2}$$

where A_i , μ_i , σ_i and ΔI are the amplitude, mean, standard deviation and change in open-pore current due to analyte translocation of the i^{th} component respectively. The histograms corresponding to change in open-pore current due to hSTf translocation (Figure S9) were fitted using a bimodal Gaussian mixture model (GMM) with each in the form of Eq. S2 using the in-built *FindDistributionParameters* function of Mathematica 11.0.1.0. The two peaks of the fit were assigned as $\Delta I_{p,c}$ and $\Delta I_{p,f}$ respectively in order of increasing ΔI . The $\Delta I_{p,c}$ was attributed to the unfolded conformation whereas $\Delta I_{p,f}$ to the pseudo-folded conformation. The term pseudo-folded was coined since the conformation would be deviated from the native globular state due to voltage application. The $\Delta I_{p,c}$ and $\Delta I_{p,f}$ can be translated into change in conductance components ($\Delta G_{p,c}$ and $\Delta G_{p,f}$ respectively) by dividing each from the appropriate applied voltage.

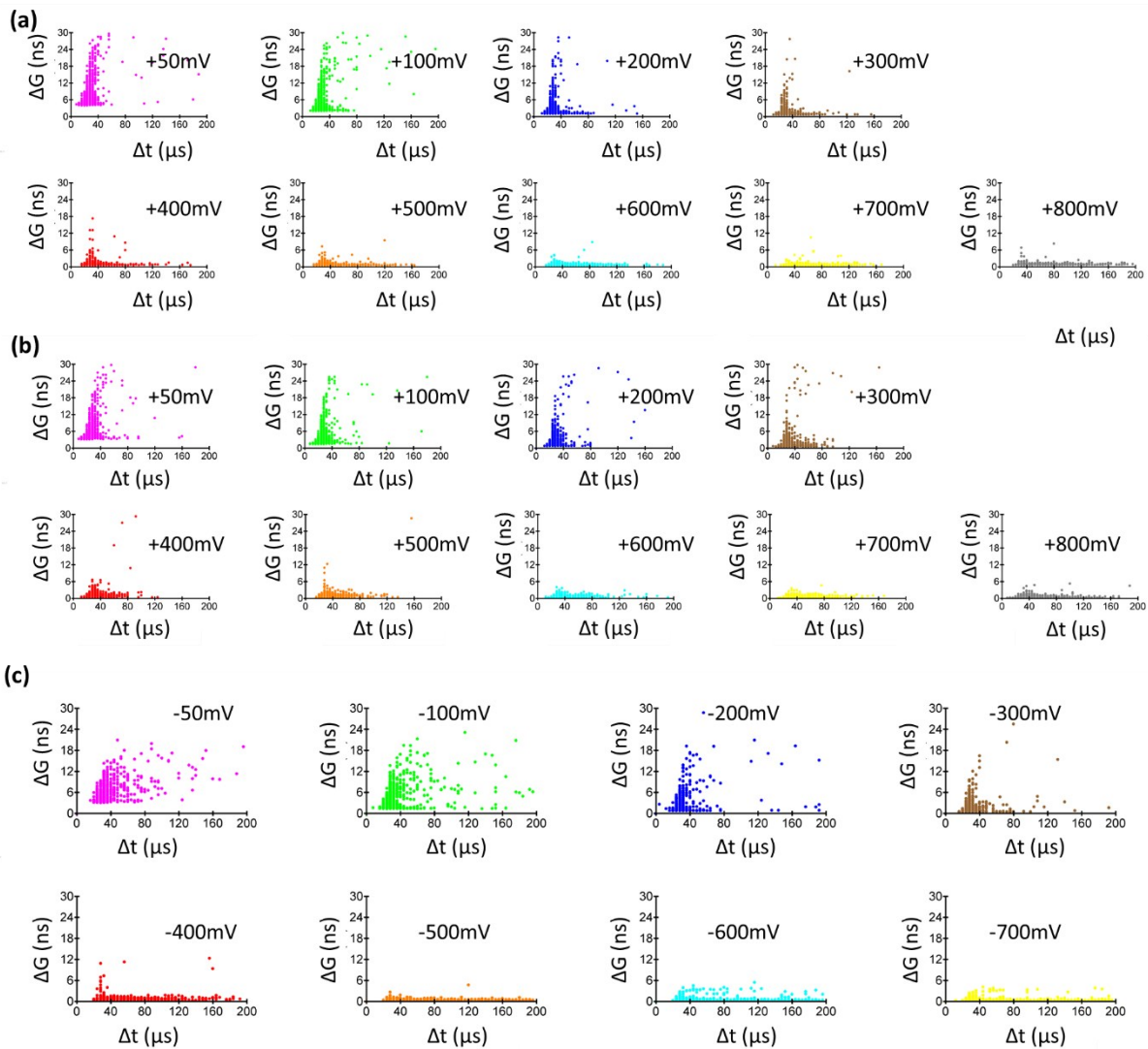


Figure S8: Scatter Plots of change in conductance vs translocation time corresponding to (a) 2M KCl, (b) 4M LiCl, and (c) 1 M LiCl at applied voltages indicated in each panel. All experiments were carried out at pH~8 using ~14 nm diameter nanopores.

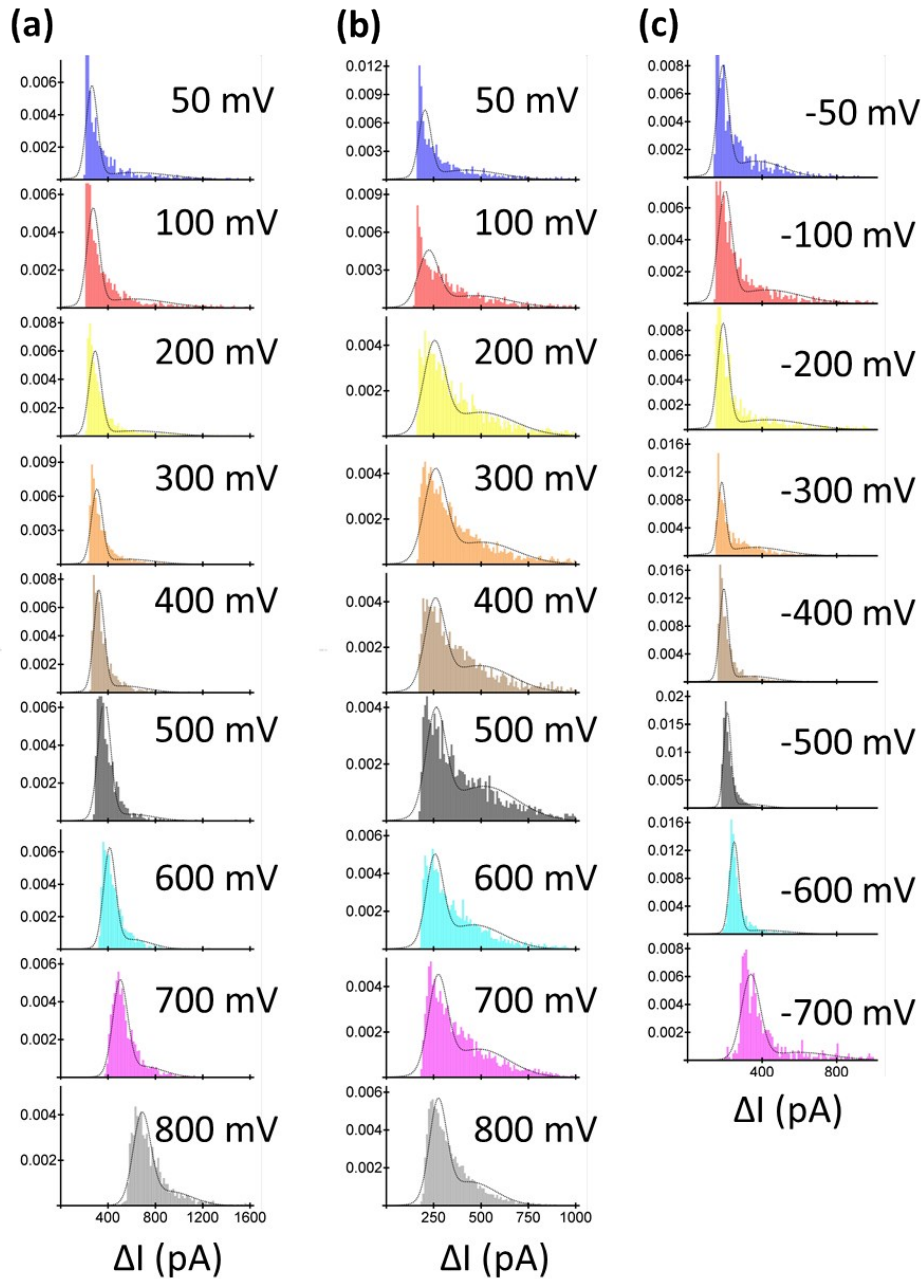


Figure S9: Histograms and the corresponding Gaussian mixture model (GMM) fits corresponding to change in conductance as a result of hSTf translocation in **(a)** 2M KCl, **(b)** 4M LiCl and **(c)** 1M LiCl. The y axis represents normalized counts. All experiments were carried out pH~8 using ~14 nm diameter nanopores.

Section 4: ζ_{pore} , σ_{hSTf} and Electrolyte Concentration

The surface charge density (σ_p) of the nanopore is tightly correlated with EO and can be

approximated as $|\sigma_p| \cong \frac{C_{eff}}{\beta e} W\left(\frac{\beta_T e}{C_{eff}} \exp((pH - pK_a) \ln(10) + \ln\left(\frac{10}{\beta_T e}\right) e\Gamma)\right)$, where W , C_{eff} , e , β_T , pK_a are the

Lambert W function, effective Stern layer capacitance, elementary charge, inverse of thermal energy and $-\log$ of the dissociation constant of the surface chargeable head group, respectively.²

The surface parameters are also sensitive to electrolyte composition and Grahame's equation

captures this dependence through $\sigma_p = \frac{2\epsilon_r\epsilon_0\kappa}{\beta e} \sinh\left(\frac{\beta e\phi_{pore}}{2}\right)$ where $\epsilon_r\epsilon_0$, ϕ_{pore} and κ are the permittivity

of the solution, the surface potential of the pore and Debye screening length, respectively. Debye

length (κ^{-1}) can be calculated from $\kappa^2 = \frac{\beta e^2 n_{MX}}{\epsilon_r\epsilon_0}$ where n_{MX} is the numerical concentration of the

electrolyte MX.³⁻⁵ It is somewhat customary to assume $\phi_{pore} \approx \zeta_{pore}$ where ζ_{pore} is the zeta potential

of the nanopore surface.^{3,6} For lower potentials, Grahame equation can be approximated to

$$\zeta_{pore} = \frac{\sigma_p}{\epsilon_r\epsilon_0} \kappa^{-1} \quad \text{Eq. S3}$$

since

$$\sinh\left(\frac{\beta e\zeta_{pore}}{2}\right) = \frac{\beta e\zeta_{pore}}{2} + \frac{\left(\frac{\beta e\zeta_{pore}}{2}\right)^3}{3!} + \dots \sim \frac{\beta e\zeta_{pore}}{2} \quad \text{Eq. S4}$$

since κ^{-1} and n_{MX} have an inverse relationship, as electrolyte concentration decreases, κ^{-1} would increase and thereby ζ_{pore} would increase too for a given operational pH. Therefore, when the electrolyte concentration is low enough to satisfy the $\zeta_{hSTf} < \zeta_{pore}$ condition, the hSTf translocation

would be EO-dominant and events would be observed for negative voltage polarities instead of positive polarities.

	C (M)	0.5	1	1.5	2	2.5	3	4
LiCl	ξ_{pore} (mV)	-52.3±3.8	-37.0±2.7	-30.2±2.2	-26.1±1.9	-23.4±1.7	-21.4±1.6	-18.6±1.3
KCl	ξ_{pore} (mV)	-50.5±5.9	-35.7±4.2	-29.1±3.4	-25.2±3.0	-22.6±2.6	-20.6±2.4	-17.9±2.1

Table S1: Zeta potential of the nanopore surface (ξ_{pore}) calculated using Eq. S3 through σ_p obtained using open-pore conductance surveying using LiCl and KCl.

Electrolyte	Zeta Potential (mV)
50 mM LiCl	-4.7±0.8
50 mM KCl	-6.2±1.3
KCl at 50 mM LiCl conductivity	-5.6±0.8

Table S2: The zeta potential measured using the Zetasizer in 50 mM LiCl, 50 mM KCl and KCl with conductivity equivalent to 50 mM LiCl.

Section 5: Quantification of Capture Rate

The three commonly used methods for quantification of capture rate are i) averaged inter-event time, ii) events per unit time, and iii) slope of events versus absolute time. Since there is some latent time before event frequency reaches its maximum value, calculation of (i) or (ii) would lead to a considerable standard deviation of the averaged values. However, this variability could be easily reduced through approach (iii) as the plot would show the lag phase clearly through a slow increase in event count with time and; once the capture rate reaches its optimal value, the event count would increase linearly with time. The slope of this phase is taken and presented as the capture rate.

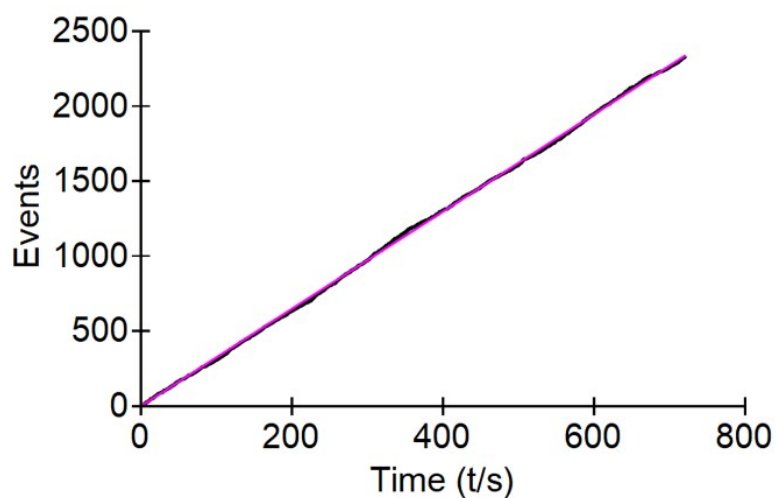


Figure S10 : Event count with absolute time. The magenta line is a linear fit made to the data shown in black.

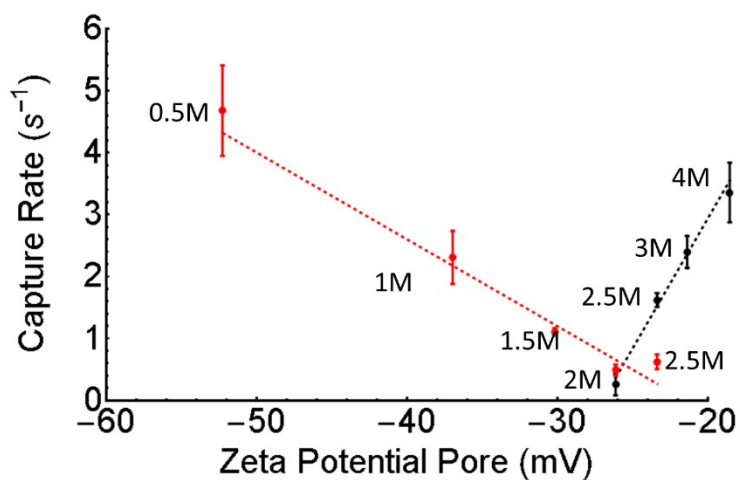


Figure S11: Event rate of hSTf in 4 M to 0.5M LiCl in response to +50 mV (black) and -50 mV (red). Experiments were conducted at pH ~8 using ~14 nm diameter and the solid lines are a linear fit to the raw data.

Section 6: Derivation of Equation 5

Change in bulk resistance (ΔR) due to the passage of a sphere with a radius r_p , through a channel with length L and radius r_0 filled with an electrolyte with a conductivity of K is given by,⁷

$$\Delta R = \frac{2r_p^3}{K\pi r_0^4} \quad \text{Eq. S5}$$

Therefore, the conductance change of the bulk component, $\Delta G_{B,P}$ will be,

$$\Delta G_{B,P} = K \frac{\pi r_0^4}{2r_p^3} \quad \text{Eq. S6}$$

For a channel with length L and radius r_0 , the open-channel conductance ($G_{channel}$) while considering the end effect is given by,⁸

$$G_{channel} = K \frac{\pi r_0^2}{(L + 1.6r_0)} \quad \text{Eq. S7}$$

Dividing Eq. S6 from Eq. S7 leads to,

$$\frac{\Delta G_{B,P}}{G_{channel}} = \frac{2r_p^3}{(L + 1.6r_0)r_0^2} \quad \text{Eq. S8}$$

Thus,

$$\Delta G_{B,P} = \frac{2r_p^3}{(L + 1.6r_0)r_0^2} G_{channel} \quad \text{Eq. S9}$$

Substituting Eq. S7 to Eq. S9,

$$\Delta G_{B,P} = \frac{2r_p^3}{(L + 1.6r_0)r_0^2} \cdot K \frac{\pi r_0^2}{(L + 1.6r_0)} \quad \text{Eq. S10}$$

$$\Delta G_{B,P} = K \frac{2\pi r_p^3}{(L + 1.6r_0)^2} = K \frac{2 \cdot \frac{4}{3}\pi r_p^3}{4/3(L + 1.6r_0)^2} = K \frac{1.5 \cdot \Lambda}{(L + 1.6r_0)^2} = K \frac{\gamma \cdot \Lambda}{(L + 1.6r)^2} \quad \text{Eq. S11}$$

The assignment of 1.5 for γ for a sphere arises from Eq. S11.

The fundamental problem with using this equation for a nanopore lies with Eq. S7 which is derived for a micron-scale tube. However, for a nanopore, the open pore conductance is given by

$$G_{nanopore} = K \left(\frac{1}{\frac{\pi r_0^2}{L} + \frac{\mu|\sigma|}{K} \cdot \frac{2\pi r_0}{L}} + \frac{2}{\alpha \cdot 2r_0 + \beta \cdot \frac{\mu|\sigma|}{K}} \right)^{-1} = \left(\frac{1}{G_{bulk} + G_{surface}} + \frac{1}{G_{access}} \right)^{-1} \quad \text{Eq. S12}$$

S12

Unlike DNA, proteins do not have a uniform charge and the shape is dependent on a host of factors. Therefore, estimation of charge as a function of its geometry requires computations outside the scope of this study. Thus, in this work we neglect any contributions from the surface charge of proteins. Given this approximation, conductance change as a result of protein confinement can be written as,

$$\Delta G_p = G - \left(\frac{1}{G_{bulk} + G_{surface}} + \frac{1}{G_{access}} \right)^{-1} \quad \text{Eq. S13}$$

G_{bulk} is the bulk conductance as a result of the protein confinement which can be written as,⁷

$$G_{bulk} = K_{eff} \frac{\pi r_0^2}{L} \quad \text{Eq. S14}$$

where K_{eff} the effective conductivity. Using Maxwell's approximation, K_{eff} can be written in terms

of volume fraction (f) of an insulating sphere $\left(\frac{4r_p^3}{3r_0^2L}\right)$ in a solution with conductivity, K can be expressed as,⁹

$$K_{eff} = \frac{K}{\left(1 + \frac{3}{2}f + \dots\right)} \quad \text{Eq. S15}$$

Thus,

$$G_{bulk} = \frac{K}{\left(1 + \frac{3}{2}f + \dots\right)} \frac{\pi r_0^2}{L} \quad \text{Eq. S16}$$

Thus using Eq. S13 through Eq. S16, the ΔG_p can be expressed as

$$\Delta G_p = G - K_{eff} \left(\frac{1}{\frac{\pi r_0^2}{L} + \frac{\mu|\sigma|}{K_{eff}} \cdot \frac{2\pi r_0}{L}} + \frac{2}{\alpha \cdot 2r_0 + \beta \cdot \frac{\mu|\sigma|}{K_{eff}}} \right)^{-1} \quad \text{Eq. S17}$$

We note, considering the nanopore to be an ionic conductor (where in-series and parallel resistance contributions must be considered appropriately as outlined in Eq. S17), the drop in one component does not contribute in the same magnitude to the drop in the total resistance of the pore. Therefore, the linear addition of contributions for the final $\Delta G_{p,f}$ must be done with utmost diligence. That is, if ΔG due to physical blockage of the nanopore volume from the analyte is $\Delta G_{b,a}$, and nanopore surface charge and particle are $\Delta G_{s,np}$ and $\Delta G_{s,a}$ respectively, then total change in conductance, $\Delta G_{p,f} \neq \Delta G_{b,a} + \Delta G_{s,np} + \Delta G_{s,a}$ rather $\Delta G_{p,f} = \Delta G_{b,a} // (\Delta G_{s,np} // \Delta G_{s,a})$ where '//' indicate parallel ionic resistor contributions. For simplicity, we would only consider the first six terms of the volume fraction and neglect contributions from the protein charge.

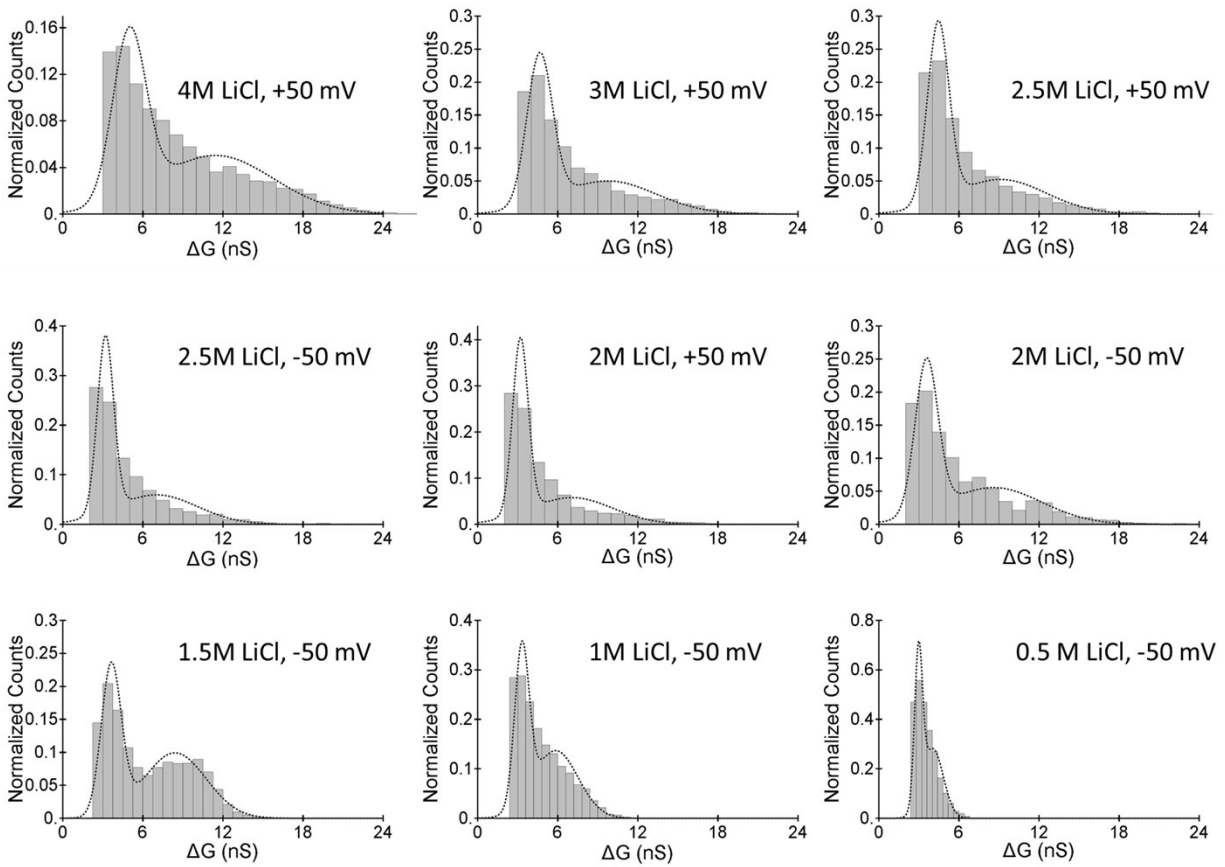


Figure S12 :Histograms corresponding to the change in conductance originating from translocation of hSTf (scatter plots shown in Figure S5) under experimental conditions outlined in respective legends.

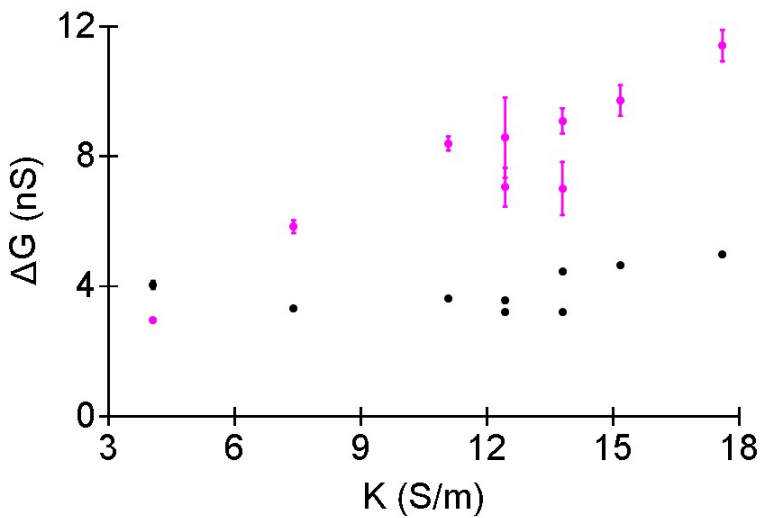


Figure S13: The ΔG with LiCl conductivity corresponding to distributions shown in Figure S12 with black and magenta points representing $\Delta G_{p,c}$ and $\Delta G_{p,f}$ respectively.

References

1. Pedone, D.; Firnkes, M.; Rant, U., Data analysis of translocation events in nanopore experiments. *Anal. Chem.* **2009**, *81*, 9689-9694.
2. D. Y. Bandara, Y. M. N.; Saharia, J.; Karawdeniya, B. I.; Hagan, J. T.; Dwyer, J. R.; Kim, M. J., Beyond nanopore sizing: improving solid-state single-molecule sensing performance, lifetime, and analyte scope for omics by targeting surface chemistry during fabrication. *Nanotechnology* **2020**, *31*, 335707.
3. Arjmandi, N.; Van Roy, W.; Lagae, L.; Borghs, G., Measuring the electric charge and zeta potential of nanometer-sized objects using pyramidal-shaped nanopores. *Anal. Chem.* **2012**, *84*, 8490-8496.
4. Smeets, R. M.; Keyser, U. F.; Krapf, D.; Wu, M.-Y.; Dekker, N. H.; Dekker, C., Salt dependence of ion transport and DNA translocation through solid-state nanopores. *Nano Lett.* **2006**, *6*, 89-95.
5. Frament, C. M.; Bandara, N.; Dwyer, J. R., Nanopore surface coating delivers nanopore size and shape through conductance-based sizing. *ACS Appl. Mater. Interfaces* **2013**, *5*, 9330-9337.
6. Kejian, D.; Weimin, S.; Haiyan, Z.; Xianglei, P.; Honggang, H., Dependence of zeta potential on polyelectrolyte moving through a solid-state nanopore. *Appl. Phys. Lett.* **2009**, *94*, 014101.
7. DeBlois, R.; Bean, C., Counting and sizing of submicron particles by the resistive pulse technique. *Rev. Sci. Instrum.* **1970**, *41*, 909-916.
8. Ito, T.; Sun, L.; Crooks, R. M., Simultaneous determination of the size and surface charge of individual nanoparticles using a carbon nanotube-based Coulter counter. *Anal. Chem.* **2003**, *75*, 2399-2406.
9. Maxwell, J. C., *A treatise on electricity and magnetism*. Oxford: Clarendon Press: 1873; Vol. 1.